AIP | Physics of Fluids

Threshold criteria for incipient sediment motion on an inclined bedform in the presence of oscillating-grid turbulence

W. H. M. Wan Mohtar and R. J. Munro

Citation: Physics of Fluids **25**, 015103 (2013); doi: 10.1063/1.4774341
View online: http://dx.doi.org/10.1063/1.4774341
View Table of Contents: http://scitation.aip.org/content/aip/journal/pof2/25/1?ver=pdfcov
Published by the AIP Publishing

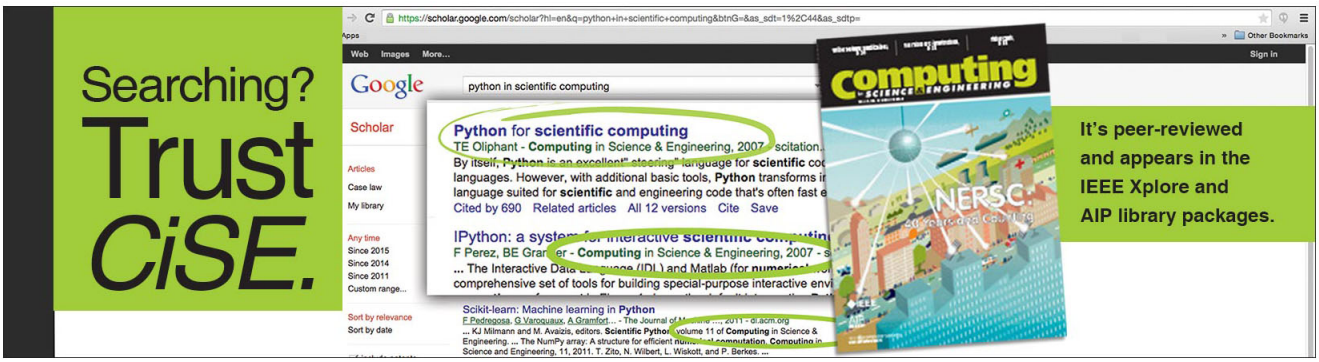

PHYSICS OF FLUIDS **25**, 015103 (2013)

Threshold criteria for incipient sediment motion on an inclined bedform in the presence of oscillating-grid turbulence

W. H. M. Wan Mohtar[1,2] and R. J. Munro[1]
[1]*Faculty of Engineering, University of Nottingham, Nottingham NG7 2RD, United Kingdom*
[2]*Department of Civil and Structural Engineering, Faculty of Engineering and Built Environment, Universiti Kebangsaan Malaysia, 43650 B. B. Bangi, Malaysia*

(Received 28 June 2012; accepted 6 December 2012; published online 14 January 2013)

Here, we report laboratory experiments to investigate the threshold criteria for incipient sediment motion in the presence of oscillating-grid turbulence, with the bed slope inclined at angles between the horizontal and the repose limit for the sediment. A set of nine mono-disperse sediment types was used with size ranges normally associated with either the hydraulically-smooth or transitional regimes. Measurements of the (turbulent) fluid velocity field, in the region between the grid and bedform's surface, were obtained using two-dimensional particle imaging velocimetry. Statistical analysis of the velocity data showed that the turbulence had a anisotropic structure, due to the net transfer of energy from the normal to the tangential velocity components in the near-bed region, and that the fluctuations were dominant compared to the secondary mean flow. The sediment threshold criteria for horizontal bedforms were compared with, and found to be in good qualitative agreement with the standard Shields curve. For non-horizontal bedforms, the bed mobility was found to increase with increasing bed slope, and the threshold criteria were compared with previously-reported theoretical models, based on simple force-balance arguments. © *2013 American Institute of Physics*. [http://dx.doi.org/10.1063/1.4774341]

I. INTRODUCTION

Models used to estimate bedload-sediment-transport rates often rely on a prediction of the threshold (or critical) conditions required to induce incipient sediment motion. Since the seminal work of Shields,[1] (published in 1936), practitioners have relied almost exclusively on some form of the Shields[1] diagram for estimating these threshold criteria in unidirectional flows: in essence, the Shields[1] diagram relates the threshold conditions for a grain of nominal diameter D to the dimensionless Shields[1] parameter $\tau_c/(\rho_s - \rho)gD$, where ρ_s and ρ are the densities of the sediment and fluid, respectively, and τ_c is the critical bed shear stress. However, the results of Shields,[1] and many of the experimental studies[2–5] that have since provided validation of the Shields[1] diagram, are based on data obtained using shallow-sloped, uniform steady channel flows. Under these idealised, statistically stationary conditions, the near-bed turbulent fluctuations that give rise to the hydrodynamic forces that induce sediment motion are correlated with the time-averaged mean flow speed. As a result, it is typical for standard sediment-transport models to be parameterised in terms of mean flow characteristics, such as the time-averaged mean bed shear stress, with the effects due to turbulent fluctuations considered implicitly.

However, naturally occurring flows are often neither uniform, nor statistically stationary, with the near-bed turbulence intensity varying significantly with bed position and time. Typical factors causing this non-uniformity and/or intermittency can include local variations in bed slope or bed geometry,[6,7] obstacles within the flow,[8] and the presence or development of intermittent coherent vortex structures in the near-bed region.[9–12] Under these conditions, the near-bed turbulence is no longer necessarily correlated with the mean flow characteristics, and so the parametric relations for

sediment transport quantities, based on steady uniform flows, can often provide poor comparisons with experiment data.[8]

As noted by Schmeeckle *et al.*,[13] improvements in our understanding of the sediment transport process, in general, requires a detailed knowledge of how turbulent fluctuations in the near-bed region interact with and displace sediment grains. Attempts have been made to address this issue using novel experiments performed in steady channel flows: See, for example, the channel-flow experiments reported by Sumer *et al.*[8] who used an array of grids placed at different heights along the channel to vary the near-bed turbulence intensity. However, it is also necessary for researchers to consider different types of turbulent flow, with attention focussed on the role played by turbulent fluctuations. The experiments described in this article attempt to address this issue and report measurements of sediment threshold-criteria obtained in the presence of a class of stationary turbulence, which is effectively free of a mean flow, thereby allowing the affect of turbulent fluctuations to be considered in isolation.

The validity of the Shields[1] diagram is also restricted to horizontal or shallow-sloped bedforms, and comparatively few studies have examined how sediment threshold-criteria are affected by non-negligible increases in bed slope. [See the meta analysis by Lamb *et al.*[14] for a broad overview of experimental studies focussed on bed-slope effects.] Previous theoretical studies,[14,15] based on force-balance arguments, have derived models that predict a sediment bed's mobility increases with bed slope, due to the increased down-slope component of gravitational acceleration acting on the constituent sediment grains. Despite this, data from both field and laboratory studies have been reported that indicate the opposite trend,[14] suggesting that significant increases in bed slope act to stabilise the bed. Of course, when the bed slope in a open-channel flow becomes relatively steep, uniform flow conditions are difficult to achieve, and the flow is likely to become supercritical. Indeed, Lamb *et al.*[14] attribute the counter-intuitive measurements to how the structure of the near-bed turbulence in an open-channel flow is affected by the decrease in flow depth (h), and the corresponding increase in relative bed roughness z_*/h, that occurs as the bed slope is increased (where, here, z_* denotes the roughness length-scale). With this factor eliminated, experiment data have been reported that exhibit clear agreement with the increased-mobility trend predicted by the theory.[16,17]

The situation is even more complicated for the threshold conditions associated with oscillatory wave motions, where the near-bed mean flow exhibits notable periodic spatial and temporal accelerations and decelerations. In this case, the near-bed tangential flow can be characterised by the orbital diameter $d = H/\sinh(2\pi h/L)$ and the peak critical flow velocity $u_m = \pi d/T$, where h is the mean water depth and H, L, and T denote, respectively, the amplitude, length, and period of the waves. It has been reported[18] that for grain sizes smaller than about 0.5 mm, the critical conditions are achieved while the boundary layer adjacent to the bed is laminar, in which case Komar and Miller[19] showed that the dimensionless shear stress $\rho u_m^2/(\rho_s - \rho)gD$ is proportional to $(d/D)^{1/2}$. Conversely, for larger grain sizes the boundary layer is turbulent under critical conditions, and the corresponding threshold criteria can be determined using an empirical curve relating $\rho u_m^2/(\rho_s - \rho)gT$ to (d/D).[19]

This paper reports the results of experiments to examine the threshold conditions for incipient sediment motion in the presence zero-mean-shear turbulence. Here, the turbulence is generated by a uniform grid made to oscillate with constant amplitude and frequency, with the spanwise plane of the grid above and always parallel to the bed surface. The turbulence produced in this way is characterised by fluctuations that are dominant compared to the mean flow, which allows the interaction between the sediment and near-bed turbulent fluctuations to be studied. This class of "zero-mean," statistically stationary turbulence, commonly referred to as oscillating-grid turbulence (OGT), has been used previously to study, for example, isotropic homogeneous turbulence,[20,21] entrainment across a density interface,[22,23] and particle suspensions and sedimentation.[24,25]

Previous studies using OGT have also reported measurements of threshold criteria for sediment transport.[26,27] These studies considered a range of natural and artificial sediments, but did not account for (a) how the threshold criteria were affected by increases in bed-slope, or (b) how the presence of the bedform affected the statistical properties of the turbulence in the near-bed region. The experiments reported here address both of these factors. That is, measurements of threshold-criteria were obtained for a range of bed slopes between the horizontal and the sediment's repose

limit (typically 30°), and are compared with existing force-balance models derived to account for bed slope effects. In addition, time-resolved particle imaging velocimetry (PIV) was used to investigate how the statistical properties of the turbulence were affected by the presence of the sediment bed, with the threshold criteria analysed in terms of a modified critical Shields[1] parameter defined in terms of the near-bed root-mean-square (rms) velocity components.

The paper is set-out as follows. Section II describes the experiment apparatus, measurement techniques and how the OGT system was used to determine the threshold criteria. The results are given in Sec. III, and are compared with previously reported force-balance models.[16,17] Final remarks and discussions are presented in Sec. IV.

II. EXPERIMENTS

A. Apparatus

Figure 1(a) shows a sketch of the OGT system. Each experiment was performed inside an acrylic tank with square internal cross section (35.4 cm × 35.4 cm) and height 50 cm, fixed within

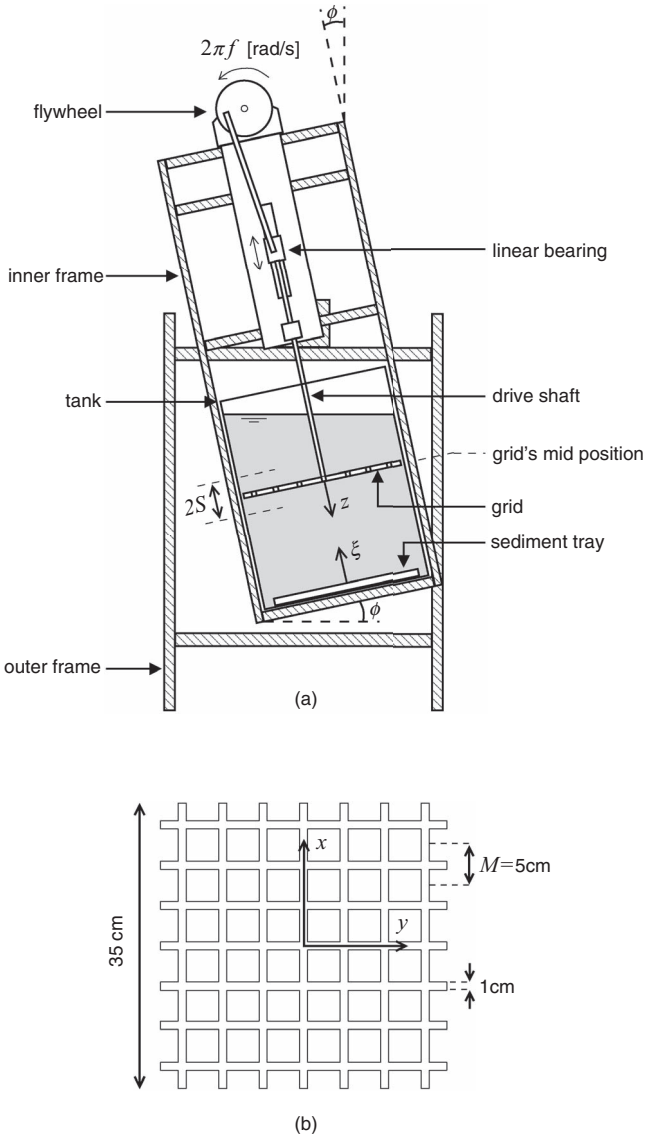

FIG. 1. Sketches showing (a) the key features experiment apparatus, and (b) a (magnified) plan-view of the grid.

a rigid inner frame and partially filled with water. The oscillating-grid mechanism consisted of a motor-driven flywheel attached to the top of the inner frame (see Fig. 1(a)), used to drive a central shaft via a crank and linear bearing, which converted the rotary motion of the flywheel to vertical oscillatory motion of the drive shaft. The turbulence-generating grid was fixed (rigidly) to the base of the drive shaft and suspended centrally inside the tank (below the water free-surface) with the spanwise plane of the grid parallel to the tank base, and with a 2 mm clearance between the grid's perimeter and sidewalls of the tank.

The underside plan-view of the square, uniform grid is shown in Fig. 1(b), and consisted of a 7×7 array of aluminum bars of square cross-section ($1\,\text{cm} \times 1\,\text{cm}$) and length 35 cm, with a uniform mesh size $M = 5\,\text{cm}$ (giving a solidity of 36%). The design of the grid's end-condition was based on previous OGT studies,[28] and manufactured so that each tank sidewall acted as a plane of reflection-symmetry, which has been shown to lessen the Reynolds-stress gradients within the fluid, thereby inhibiting the presence of secondary mean circulations (see Fernando and De Silva[28] for a detailed discussion). The stroke (S) and oscillation frequency (f) of the grid were varied by altering, respectively, the flywheel radius and the rotation rate of the motor. [Note, here, the stroke S is defined as the amplitude of oscillation about the grid's mid position (see Fig. 1).] The experiments reported here used strokes of $S = 2\,\text{cm}$ and 4 cm, with the frequency f varied between 0.5 and 6 Hz. The height of the grid's mid-position above the tank base, henceforth denoted H, could be altered by changing the length of the drive shaft.

The focus of the experiments reported here was to examine how increases in bed slope affect the threshold criteria for incipient sediment motion in the presence of OGT. It was therefore necessary that the nature of the interaction between the turbulence and the sediment bed (which was formed as a shallow layer at the base of the tank) be similar for each bed slope. This was achieved by fixing the inner frame (containing the tank and oscillating-grid mechanism) on a horizontal axle held within a rigid outer frame. The inner frame could then be rotated about the axle to set the inclination angle, ϕ, of the tank (as shown in Fig. 1(a)), while keeping the spanwise plane of the oscillating grid parallel to the tank base, and hence the surface of the sediment layer. Once set at the required inclination angle the inner frame was locked rigidly in position for the duration of the experiment. As shown in Fig. 1, we henceforth let z denote the depth normal to the grid with $z = 0$ corresponding to the grid's mid position, and (x, y) the coordinates in the spanwise plane of the grid, relative to the grid's centre.

B. The statistical properties of isotropic OGT

Before describing the properties of the sediments and how the OGT system was used to determine the sediment threshold-criteria, we first present the results of a series of preliminary experiments to test the oscillating-grid mechanism and to compare the basic statistical properties of the turbulence produced with those reported in previous studies.

The statistical properties of OGT, in a homogeneous fluid, have been studied extensively using experimental apparatus similar to those described above.[21,22,28] Within certain design restrictions (viz., grid solidity less than 40%, oscillation frequency between 0.5 and 7 Hz, the grid end-condition designed so that each tank sidewall is a plane of reflection-symmetry),[28] it has been shown that a vertically oscillating horizontal grid produces statistically stationary, zero-mean turbulence that is horizontally homogeneous at depths beyond 2 to 3 mesh widths (M) below the grid's mid position. Under these conditions, it can be shown (see, for example, Sec. 5 of Hopfinger and Toly)[23] that the decay of the time-averaged root-mean-square (rms) horizontal velocity components (u, v), with depth z below the grid's mid position, can be expressed as

$$u = v = C_1 f M^{\frac{1}{2}} S^{\frac{3}{2}} z^{-1}, \tag{1}$$

for $z \gtrsim 2.5M$, where $C_1 > 0$ is a dimensionless constant. The derivation of (1) requires the assumption that the integral length scale of the turbulence ℓ satisfies (for $z \gtrsim 2.5M$)

$$\ell = C_2 z, \tag{2}$$

where again $C_2 > 0$ is constant. [In this article, the integral length scale ℓ, following the approach adopted by Thompson and Turner,[22] was defined as the area under the auto-correlation function of the horizontal velocity component.] Data reported in a variety of previous OGT studies have been shown to be consistent with (1) and (2), where typically $0.25 \leq C_1 \leq 0.5$ and $C_2 = 0.1$.[29] Moreover, previous studies have also shown that the turbulence generated by an oscillating grid is also effectively isotropic within the homogeneous region (i.e., $z \gtrsim 2.5M$), with measured values of the isotropy parameter, w/u, approximately constant with z and typically within the range 1.1 to 1.3, where w denotes the time-averaged rms vertical velocity component.

The statistical properties of the turbulence produced by the oscillating-grid mechanism described here were measured and compared with (1) and (2). A series of test experiments was performed, each with the inner frame and tank vertical ($\phi = 0$), with no sediment present in the tank, and with the grid's mid position set at height $H = 25\,\text{cm} = 5M$, which ensured that the tank's base had no significant affect on the turbulence produced. Strokes of $S = 2\,\text{cm}$ and 4 cm were used, with the oscillation frequency f varied between 1 and 6 Hz.

Velocity measurements were obtained using two-dimensional planar PIV, applied in the vertical (x, z)-plane through the centre of the tank (at $y = 0$). Small, reflective, neutrally buoyant tracer particles were mixed thoroughly within the water volume, and illuminated using a narrow vertical light sheet directed through the tank's central plane. The motion of the tracer particles, advected by the turbulence, was recorded using a high-speed Dantec Nanosense MkIII digital camera (with 1280×1024 pixel resolution and frame rate set at 200 Hz), positioned to view horizontally through the transparent tank sidewall. In each case, the turbulence was allowed to become establish for a period of at least 5 min. prior to measurements being taken. Each of the digital images captured by the camera corresponded to a physical region of height $0 \leq z \leq H$ and width $-W \leqslant x \leqslant W$ within the central mid-plane of the tank, where $2W = 0.6L$ and $L = 35.4\,\text{cm}$ is the internal tank width. Images were acquired for a period of 120 s, and measurements of the instantaneous velocity fields were calculated from these images at the end of each experiment using standard PIV software. Post processing of the images showed that mean and rms velocity components were essentially converged after time averaging over a period of at least 80 s.

Figures 2(a) and 2(b) show, respectively, the measured values of the spatially averaged horizontal rms velocity component, $\langle u \rangle$, and integral length scale, ℓ, both plotted against depth z. [In Fig. 2(a), the data have been plotted in dimensionless form according to equation (1).] Here, the operator $\langle \cdot \rangle$ denotes the spatial average over x, defined as

$$\langle u(z) \rangle = \frac{1}{2W} \int_{-W}^{W} u(x, z)\, \mathrm{d}x. \tag{3}$$

Both plots show data from five separate experiments, each represented by a different data symbol (see caption for details). Despite general scatter, the data shown in Fig. 2 are consistent with corresponding measurements reported in previous OGT studies,[21,23,28] and are well described by the relationships defined in Eqs. (1) and (2), which are also shown (solid lines) with $C_1 = 0.34$ and $C_2 = 0.1$. Corresponding measurements of the isotropy parameter, $\langle w \rangle / \langle u \rangle$, for each of the five data sets, were all approximately constant with depth ($z \gtrsim 2.5M$) and within the range $1.1-1.4$, which again is consistent with data from previous studies. Similar test experiments were also performed with the tank inclined at angles between $\phi = 0^\circ$ and 30° but, as expected, no discernible differences in the measured statistical properties of the turbulence were evident.

C. Sediment characteristics and measurements of threshold criteria

Here, we introduce the basic properties of the sediment types used in the experiments, and describe how the oscillating-grid mechanism was used to measure the threshold criteria for each.

Nine sediment types were used throughout, each consisting of near-spherical grains. Their basic properties are listed in Table I, where s denotes relative density, D_{50} the median grain size and $C_u = \sqrt{D_{84}/D_{16}}$ the sediment gradation parameter. In each case, the constituent grains had a narrow size distribution about D_{50}, with values of C_u in the range $1.15-1.66$. The particle Reynolds

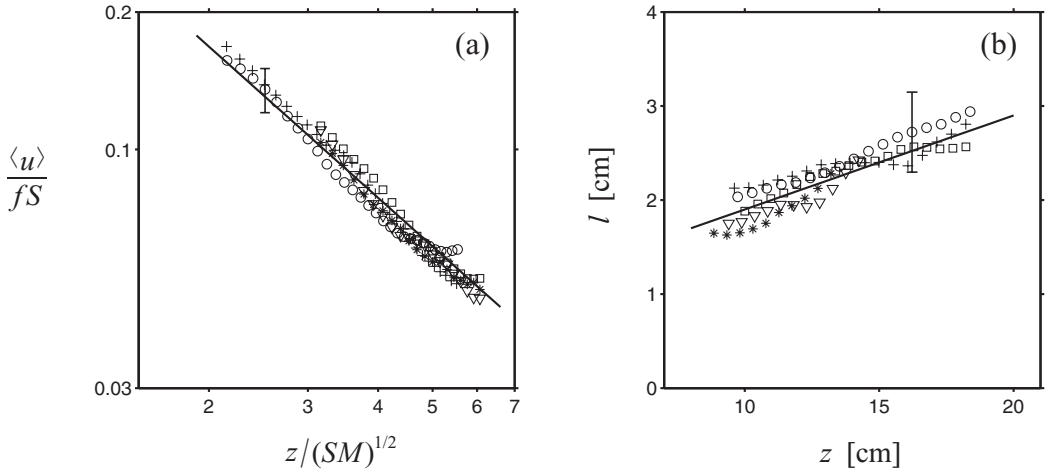

FIG. 2. Plot (a) shows the (spatially averaged) rms horizontal velocity component, $\langle u \rangle$, plotted against depth relative to the grid's mid position, z. Here, $\langle u \rangle$ and z have been made dimensionless using fS and $(SM)^{1/2}$, where recall f, S, and M are the frequency, stroke, and mesh-size of the grid, respectively. Plot (b) shows the integral length scale ℓ plotted against depth z. The experiments shown correspond to: $S = 2$ cm with $f = 1.5$ Hz (*), $f = 3.2$ ($\triangledown$), $f = 6$ Hz ($\square$); $S = 4$ cm with $f = 1.5$ Hz (+), $f = 4.8$ Hz ($\circ$). For comparison, the solid lines show Eqs. (1) and (2) with $C_1 = 0.34$ and $C_2 = 0.1$. To avoid saturation, a single error bar has been included in each plot that is representative of the variability observed in all of the data shown.

number (Re_p) is here defined as

$$Re_p = \frac{\sqrt{(s-1)g D_{50}^3}}{\nu}, \tag{4}$$

where g denotes gravitational acceleration and ν the kinematic viscosity of the fluid.

For consistency, each sediment layer was formed in a square tray of depth 1 cm and width 33 cm, clamped in position at the base of the partially filled tank, which was initially set in the vertical position ($\phi = 0$) and with the grid removed. The surface of the layer was prepared by carefully drawing a straight-edged scraper across the top rim of the tray, which produced a flat, close-packed bed of uniform depth 1 cm. The grid was then carefully reattached to the base of the drive shaft, taking care not to disturb the bedform. The bed slope could then be set by slowly tilting the inner frame (containing the tank and oscillating-grid mechanism) to the required angle ϕ, as shown in Fig. 1(a). The bed slope is henceforth denoted by $\beta \equiv \tan\phi$. To ensure that the sediment bed did not slide on the smooth tray surface when tilted, the tray base was roughened by gluing a thin layer of type A sediment to its surface.

The experiments to determine the threshold criteria for each sediment type were performed at various bed slopes within the range $0 \leq \beta < \beta_r$, where $\beta_r \equiv \tan\phi_r$ and ϕ_r denote the bed slope and

TABLE I. The important characteristics of each sediment type.

Label	Material	s	D_{50} [mm]	C_u	Re_p	ϕ_r [deg]
A	Glass	2.50	1.090	1.15	138.0	27.5
B	Glass		0.716	1.23	73.5	28.2
C	Glass		0.563	1.30	51.2	28.8
D	Glass		0.374	1.35	27.7	28.1
E	Glass		0.220	1.44	12.5	30.4
F	Glass		0.153	1.32	7.23	29.1
G	Glass		0.0801	1.66	2.74	29.0
H	Diakon	1.18	0.751	1.28	27.3	30.8
I	Diakon		0.274	1.62	6.03	33.1

bed angle at the repose limit. Note that, the repose angle (ϕ_r) for each sediment type was determined prior to the experiments using the tilting tank mechanism (with the grid and drive shaft removed), using a procedure similar to that described in Wiberg and Smith.[15] That is, with the sediment layer formed at the tank base and with the water quiescent, the tilt angle of the inner frame and tank were slowly increased from $\phi = 0$ until the bedform started to become unstable and collapse down the tray. The corresponding measured values of ϕ_r are shown in Table I, and are averages taken from several repeats (with typical variability of $\pm 2^\circ$).

To ensure that threshold conditions for each sediment type and bed slope could be induced with the grid oscillating within the operating range of frequencies (i.e., 0.5 to 6 Hz), each experiment was performed with the stroke fixed at $S = 4\,\text{cm}$ and with the grid's mid level ($z = 0$) at height $H = 17\,\text{cm} = 3.4M$ above the tank base. [Recall, in the preliminary test experiments described in Sec. II B, we used $H = 25\,\text{cm} = 5M$.] Once the sediment layer had been formed at the tank base and the bed slope set, the grid oscillation frequency (f) was incrementally increased (from zero), each time allowing the turbulence produced to become established, until a "critical" frequency was reached at which point incipient grain motion was only just induced by the turbulence interacting with the surface of the sediment bed. To minimise errors associated with identifying the threshold conditions, the procedure described above was repeated several times (for each sediment type and bed slope), so that an average value for each critical frequency, f_c, could be determined.

Once each critical frequency had been identified, measurements of the turbulence produced under these conditions, in the region between the grid and the sediment-layer surface, were obtained using the PIV set-up described above in Sec. II B. A typical set of spatially averaged rms velocity profiles obtained using this procedure are shown in Fig. 3, where $\langle u \rangle_c$ and $\langle w \rangle_c$ have been plotted against ξ, which henceforth denotes height above and normal to the sediment-layer surface (see Fig. 1(a)), and so here is shown on the vertical axis. Also, the c-subscript has been introduced to henceforth denote measurements obtained under critical (or threshold) conditions for incipient sediment motion. The normalising factors u_0, w_0, and ℓ_0 denote, respectively, the values of $\langle u \rangle_c$, $\langle w \rangle_c$, and $\langle \ell \rangle_c$ measured at depth $z = 2.5M$ (i.e., $\xi = 0.9M$). Also, shown in Fig. 3 are corresponding measurements of the turbulence intensities $\langle U \rangle_c / \langle u \rangle_c$ and $\langle W \rangle_c / \langle w \rangle_c$ plotted against ξ, where U and W denote, respectively, the time-averaged mean tangential and normal velocity components.

It is clear from Figs. 3(a) and 3(b) that the presence of the sediment layer has a significant affect on the structure of the turbulence, leading to anisotropy in the near-bed region $0 < \xi/\ell_0 \lesssim 1$. In particular, Fig. 3(b) shows that the normal rms velocity component, $\langle w \rangle_c$, decreases monotonically to zero at $\xi = 0$, due to the "blocking" effect induced by the presence of the sediment bed. In contrast, Fig. 3(a) shows that there is a notable increase observed in the tangential rms velocity component, $\langle u \rangle_c$, in the region $0 < \xi/\ell_0 \lesssim 1$, which attains a peak value, henceforth denoted by $\langle \hat{u} \rangle_c$, at around $\xi/\ell_0 = 0.3$ to 0.5, but then decreases rapidly to zero (due to viscous effects), so that the no-slip condition is satisfied at $\xi = 0$.

The structure of the turbulence evident in Fig. 3 is a result of the inter-component energy transfer produced when turbulent eddies propagate towards, and impinge with, the sediment layer.[30,31] That is, a fluid element cannot propagate through the bedform (i.e., blocking), and so an eddy moving towards the bed must turn and move parallel to the bed surface, resulting in a net transfer of energy from the normal velocity component to the tangential velocity components and, hence, in the observed peak in $\langle u \rangle_c$ near the bed surface. Note that the level of inter-component energy transfer produced by the interaction is not controlled by the "blocking" (kinematic) boundary condition on the normal velocity component, but by the viscous (dynamic) boundary condition on the tangential velocity component (through energy dissipation).[31] In addition, Figs. 3(c) and 3(d) show that the presence of the sediment layer also results in a weak secondary flow, evident by the non-zero values of the tangential (U) and normal (W) mean velocity components in the near-bed region. However, as shown, with $\langle U \rangle_c / \langle u \rangle_c$ and $\langle W \rangle_c / \langle w \rangle_c$ typically between 0.1 and 0.4, the fluctuations are always dominant compared to the mean components, and so will be the principal mechanism giving rise to sediment motion.

Under critical conditions for incipient motion, near-surface sediment grains are displaced, primarily, by the action of the hydrodynamic drag and lift forces induced across them by the tangential fluid velocity components close to the bed surface. It is standard, therefore, for sediment threshold

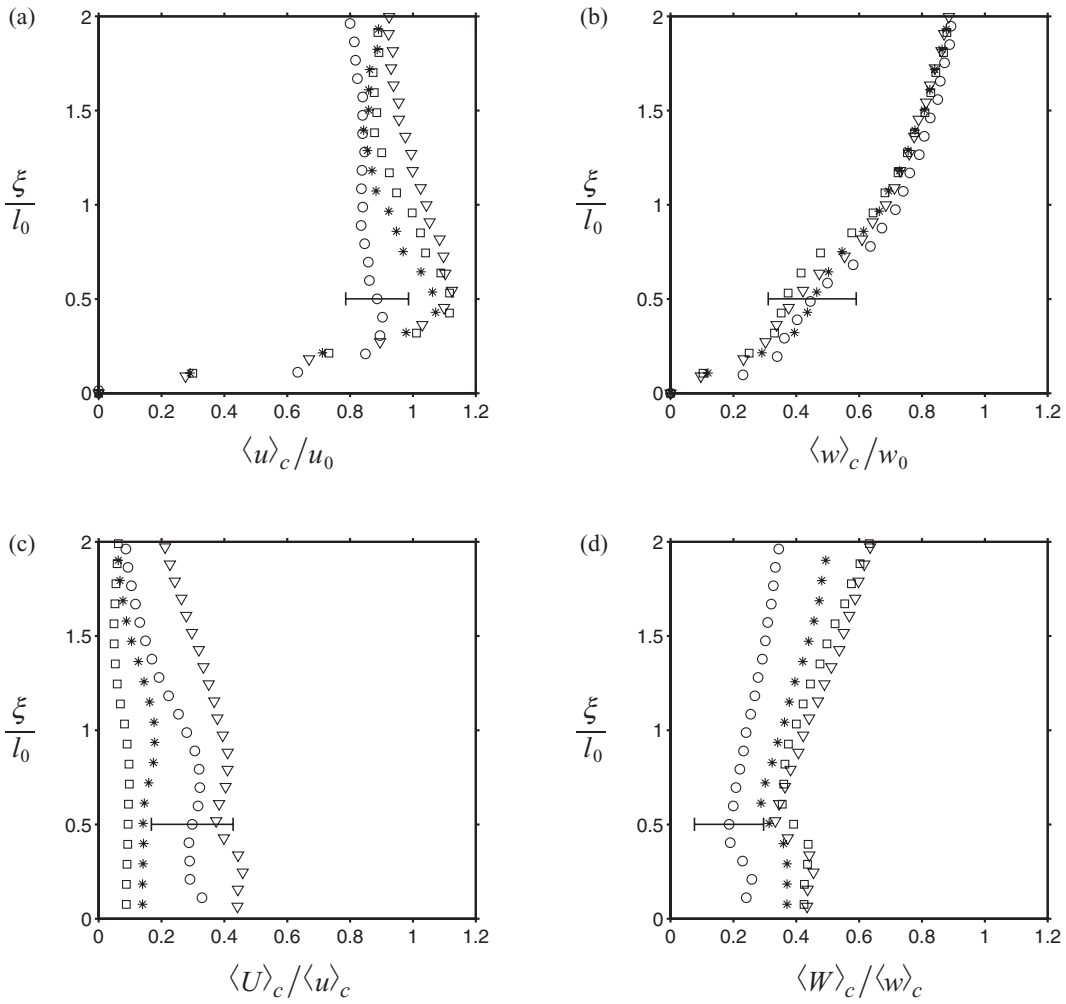

FIG. 3. Plots (a) and (b) show the measured values of the dimensionless (spatially averaged) rms horizontal, $\langle u\rangle_c/u_0$, and vertical, $\langle w\rangle_c/w_0$, velocity components against the dimensionless height relative to the sediment-bed surface, ξ/ℓ_0. Here, u_0, w_0, and ℓ_0 denote the values of $\langle u\rangle_c$, $\langle w\rangle_c$, and $\langle \ell\rangle_c$ measured at $z = 2.5M$. Plots (c) and (d) show the turbulence intensities $\langle U\rangle_c/\langle u\rangle_c$ and $\langle W\rangle_c/\langle w\rangle_c$ against dimensionless height ξ/ℓ_0. The four experiments shown correspond to: $S = 4$ cm with $f_c = 0.86$ Hz (○), $f_c = 1.7$ Hz (▽), $f_c = 2.2$ Hz (*) and $f_c = 2.3$ Hz (□). To avoid saturation, a single error bar has been included in each plot that is representative of the variability observed in all of the data shown.

criteria to be prescribed in terms of a characteristic scale for the critical bed shear stress, τ_c, below which no sediment motion is induced. In the experiments described here, it was not possible to measure τ_c directly. However, under the anisotropic conditions shown in Figs. 3(a) and 3(b), we expect the critical bed shear stress to scale as $\tau_c \sim \rho\langle\hat{u}\rangle_c^2$, where ρ denotes fluid density and, recall, $\langle\hat{u}\rangle_c$ is the peak value attained by $\langle u\rangle_c$ in the near-bed region. [Note that, the approach taken in previous studies of sediment threshold-criteria in the presence of OGT,[26,27] did not account for near-bed anisotropic conditions: In these studies, it was assumed that $\tau_c \sim \rho u^2$, with u given by Eq. (1) (which, recall, is valid only for homogeneous conditions) evaluated at the depth z corresponding to the sediment layer's surface.] For the experiments described here, the threshold conditions, for each sediment type and bed slope β (with $0 \le \beta \le \beta_r$), were here analysed in terms of a modified critical Shields[1] parameter ($\theta_{c,\beta}$), defined as

$$\theta_{c,\beta} = \frac{\langle\hat{u}\rangle_{c,\beta}^2}{(s-1)gD_{50}}, \tag{5}$$

TABLE II. A summary of the data presented in Figs. 4 and 5.

Sediment type	D_{50} [mm]	s	Re_p	ϕ_r [deg]	ϕ [deg]	$\langle \hat{u} \rangle_{c,\beta}$ [cm/s]	β/β_r	$\theta_{c,\beta}$
A	1.090	2.50	138.0	27.5	0	3.06	0.00	0.0584
					10	2.48	0.339	0.0385
					20	1.25	0.699	0.00982
					25	0.813	0.896	0.00413
B	0.716	2.50	73.5	28.2	0	2.20	0.00	0.0459
					10	1.88	0.329	0.0338
					20	1.31	0.679	0.0163
					25	0.701	0.870	0.00474
C	0.563	2.50	51.2	28.8	0	2.76	0.00	0.0919
					10	1.77	0.321	0.0378
					20	1.44	0.662	0.0249
					25	0.838	0.848	0.00852
D	0.374	2.50	27.7	28.1	0	2.09	0.00	0.0794
					10	1.47	0.339	0.0393
					20	1.19	0.699	0.0259
					25	1.02	0.896	0.0189
E	0.220	2.50	12.5	30.4	0	2.17	0.00	0.146
					10	1.71	0.300	0.0904
					20	1.43	0.620	0.0632
					25	1.18	0.795	0.0429
F	0.153	2.50	7.23	29.1	0	2.31	0.00	0.237
					10	1.80	0.317	0.144
					20	1.35	0.655	0.0808
					25	0.987	0.840	0.0432
G	0.0801	2.50	2.74	29.0	0	2.02	0.00	0.347
					10	1.45	0.317	0.178
					20	1.03	0.655	0.0902
					25	1.01	0.840	0.0870
H	0.751	1.18	27.3	30.8	0	1.26	0.00	0.120
					10	0.935	0.296	0.0862
					20	0.712	0.611	0.0499
					25	0.553	0.782	0.0301
I	0.274	1.18	6.03	33.1	0	0.819	0.00	0.139
					10	0.710	0.270	0.104
					20	0.527	0.558	0.0575

where the additional β-subscript is henceforth used to denote a quantity measured at a given bed slope β. The measured values of $\langle \hat{u} \rangle_{c,\beta}$ and $\theta_{c,\beta}$, for each sediment type and normalised bed slope β/β_r, are presented in Table II. These data are now analysed and compared with force-balance models for threshold criteria, which account for bed-slope effects.

III. RESULTS

Previous studies have derived theoretical expressions to account for how increases in bed slope affect sediment threshold criteria.[15–17] These models are based on simple force-balance arguments applied to a sediment grain (assumed spherical) situated at the surface of the bedform, and exposed to

the combined effects of (a) the hydrodynamic drag (F_D) and lift (F_L) forces that arise due to the local fluid flow over the grain, (b) the down-slope and normal components of the grain's submerged weight (W), and (c) the frictional contact forces from adjacent sediment grains. Under these conditions, the criterion for incipient grain motion, on a sediment layer inclined at some angle ϕ ($<\phi_r$) to the horizontal, can be written as (for example, see Chiew and Parker[16])

$$\beta_r = \frac{W \sin\phi + F_D}{W \cos\phi - F_L}, \tag{6}$$

where, recall, $\beta_r = \tan\phi_r$ is the bed slope at the repose angle: That is, in the absence of flow (so that $F_D = 0$, $F_L = 0$) sediment motion occurs only when the bedform is inclined at the repose angle, $\phi = \phi_r$.

The hydrodynamic drag and lift forces in Eq. (6) are commonly expressed in terms of the critical bed shear stress, i.e., $F_D,\ F_L \sim D_{50}^2\tau_c$. However, the magnitude of τ_c, and hence F_D and F_L, will also depend upon the relative roughness of the sediment layer.[15] That is, when the bedform is hydraulically rough (where, typically, $D_{50} \gtrsim 3$ mm in a steady channel flow over natural sediment),[14] the bed roughness inhibits the formation of a viscous sublayer, and so the surface sediment grains are exposed to the near-bed turbulence. For the flow considered in this article, we expect that, in this case, the peak values of the near-bed turbulence tangential to the bed surface to scale with $\langle\hat{u}\rangle_{c,\beta}$, and the corresponding characteristic scale for the critical bed shear stress to be $\tau_c \sim \rho\langle\hat{u}\rangle_{c,\beta}^2$, so that $(F_D,\ F_L) = (C_D, C_L)\pi\rho D_{50}^2\langle\hat{u}\rangle_{c,\beta}^2/2$, where C_D and C_L are drag and lift coefficients. Under these conditions, when the above expressions for F_D and F_L are substituted into Eq. (6) and combined with Eq. (5), and noting that a spherical grain has submerged weight $W = \pi(s-1)\rho g D_{50}^3/6$, it can be shown that

$$\frac{\theta_{c,\beta}}{\theta_{c,0}} = \left(1 - \frac{\beta}{\beta_r}\right)\cos\phi, \tag{7}$$

where $\theta_{c,0}$ denotes the critical Shields[1] parameter when the bedform is horizontal ($\beta = 0$). [A detailed derivation of Eq. (7) can be found in Chiew and Parker[16] (Sec. 3), or Munro[17] (Sec. III B).]

Alternatively, when the bedorm is hydraulically smooth, which for a steady channel flow over natural sediment typically corresponds to $D_{50} \lesssim 0.3$ mm,[3] a laminar viscous sublayer forms in the fluid immediately above the bed surface, within which viscous stresses act to reduce the local fluid velocities over (and around) the exposed surface-grains. (Note that this criterion on the grain size for smooth bedforms is comparable to that reported for the threshold conditions in oscillatory flows with the boundary layer adjacent to the bed being laminar—namely that the grain size is less than 0.5 mm.)[19] For the flow considered here, following the arguments used by Munro,[17] we expect the viscous-sublayer thickness and the local peak scale for the tangential fluid velocity in this case to be, respectively, of the orders $(\nu/\langle\hat{u}\rangle_{c,\beta})$ and $(D_{50}\langle\hat{u}\rangle_{c,\beta}^2/\nu)$, and for the corresponding critical bed shear stress to be $\tau_c \sim \rho D_{50}^2\langle\hat{u}\rangle_{c,\beta}^4/\nu^2$, so that $(F_D, F_L) = (C_D, C_L)\pi\rho D_{50}^4\langle\hat{u}\rangle_{c,\beta}^4/2\nu^2$. Hence, for the hydraulically smooth regime the corresponding condition takes the form

$$\frac{\theta_{c,\beta}}{\theta_{c,0}} = \left[\left(1 - \frac{\beta}{\beta_r}\right)\cos\phi\right]^{\frac{1}{2}}, \tag{8}$$

where, again, a detailed derivation can be found in Sec. III B of Munro.[17] Note that, for the experiments reported here, δ/D_{50} was found to range between 0.3 and 1.2, where $\delta = \nu/\langle\hat{u}\rangle_{c,\beta}$ denotes the characteristic thickness of the viscous sublayer. It is also worth noting that Eqs. (7) and (8) are consistent with the expected behaviour that $\theta_{c,\beta} \to \theta_{c,0}$ as $(\beta, \phi) \to 0$, and that $\theta_{c,\beta} \to 0$ as $(\beta, \phi) \to (\beta_r, \phi_r)$. Moreover, both formulae predict that the mobility of a bedform increases with bed slope. Comparing (7) and (8) also shows that the viscous damping associated with the formation of a viscous sublayer (when the bed is hydraulically smooth) acts as a stabilising influence to reduce the rate at which bed mobility increases with bed slope (in comparison to when the bedform is hydraulically rough).[17]

Equations (7) and (8) suggest that, provided $\theta_{c,0}$ is known or can be predicted (say, from the Shields[1] curve), then $\theta_{c,\beta}$, for bed slopes between $0 < \beta < \beta_r$, can be determined, in addition, from the geometric properties of the bedform (namely, β, β_r, and $\cos\phi$). Hence, before comparing the

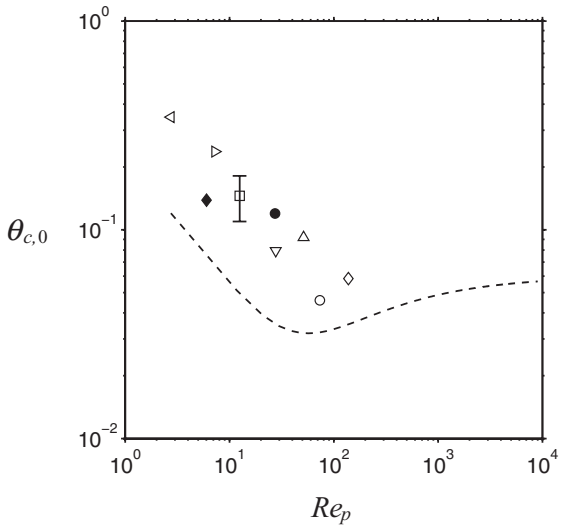

FIG. 4. Log-scale plot showing the measured values of modified Shields[1] parameter, $\theta_{c,0}$, against particle Reynolds number, $Re_p = \sqrt{(s-1)gD_{50}^3}/\nu$, for each of the nine sediment types: A (◊), B (○), C (△), D (▽), E (□), F (▷), G (◁), H (●), and I (♦). The broken-line curve shows the empirical form of the Shields[1] curve given by Eq. (9). To avoid saturation, a single error bar has been included that is representative of the variability observed in all data shown.

measured values of $\theta_{c,\beta}$ with (7) and (8), it is informative to first focus attention on the measurements of $\theta_{c,0}$, which for each of the nine sediments types used here are plotted in Fig. 4 against $Re_p = \sqrt{(s-1)gD_{50}^3}/\nu$. Each sediment type is represented by a different data symbol (see caption for details). For comparison, the standard Shields[1] curve is shown by the broken line, which has been calculated here using the empirical function

$$\theta_{c,0} = 0.22Re_p^{-0.6} + 0.06\exp\left(-17.77Re_p^{-0.6}\right), \tag{9}$$

proposed by Brownlie,[5] and recall is based primarily on measurements taken in steady open channel flows. Note that, for hydraulically rough beds (typically $Re_p \gtrsim 500$), Eq. (9) approaches a constant value of around 0.056, whereas for hydraulically smooth beds ($Re_p \lesssim 80$), the curve increases monotonically with decreasing Re_p. The region between these two cases (for $80 \lesssim Re_p \lesssim 500$) is commonly referred to as the transition region (or transitional regime). Table II suggests that, with values of Re_p between 2.7 and 140, the conditions considered here correspond to either hydraulically smooth, or transitional regimes. Referring to Fig. 4 shows that, within general scatter, the measured values of $\theta_{c,0}$ reported here are qualitatively consistent with the trend predicted by the standard Shields[1] curve defined in Eq. (9), for the range corresponding to hydraulically smooth and transitional regimes. Hence, although the properties of the turbulence considered here are significantly different from those observed in steady open channel flows, the measurements of $\theta_{c,0}$ are remarkably consistent with corresponding data reported from channel-flow studies. Clearly, Eq. (9) under predicts the measured values of $\theta_{c,0}$, although this is not surprising given the simplified expression used for the critical bed shear stress (i.e., $\tau_c \sim \rho\langle\hat{u}\rangle_{c,0}^2$) in our definition of $\theta_{c,0}$ in Eq. (5). Alternatively, we could have used $\tau_c = k\rho\langle\hat{u}\rangle_{c,0}^2$, where k is a scale factor which, in general, one would expect to be a function of Re_p and the grid Reynolds number ($Re = SMf/\nu$). However, the data in Fig. 4 suggest that the measured values of $\theta_{c,0}$, for the range of Re_p considered here, exhibit a good degree of correspondence with Eq. (9) with a scale factor of $k \approx 0.5$ (and constant).

We now focus attention on the measured values of $\theta_{c,\beta}$ for bed slopes $0 < \beta < \beta_r$. First note that, from Eq. (5), we can write $\theta_{c,\beta}/\theta_{c,0} = \langle\hat{u}\rangle_{c,\beta}^2/\langle\hat{u}\rangle_{c,0}^2$, and so following the approach adopted by Chiew and Parker,[16] Eqs. (7) and (8) can be rewritten, respectively, as

$$\frac{\langle\hat{u}\rangle_{c,\beta}}{\langle\hat{u}\rangle_{c,0}} = \left[\left(1 - \frac{\beta}{\beta_r}\right)\cos\phi\right]^{\frac{1}{2}} \tag{10}$$

and

$$\frac{\langle \hat{u} \rangle_{c,\beta}}{\langle \hat{u} \rangle_{c,0}} = \left[\left(1 - \frac{\beta}{\beta_r} \right) \cos \phi \right]^{\frac{1}{4}}, \tag{11}$$

which correspond, respectively, to the hydraulically rough and hydraulically smooth regimes. Chiew and Parker[16] compared (a form of) Eq. (10) with measurements of threshold criteria taken in a steady turbulent flow within an inclined closed conduit, using five different sediment types with grain sizes in the range 0.5 mm to 2.7 mm (which correspond to hydraulically rough beds), and with the streamwise bed slope varied between $0 \leq \beta/\beta_r \leq 0.85$. They reported measured values of $u_{*,c}/u_{*,c,0}$, where $u_{*,c} = \sqrt{\tau_c/\rho}$ is the critical bed shear velocity (evaluated using a standard empirical formula), which were shown to be in very good agreement with the right-hand-side (rhs) of Eq. (10). Munro[17] also studied bed-slope affects on threshold criteria by examining the unsteady interaction between an isolated vortex ring and a planar sediment layer (in a body of water which was otherwise quiescent). The bed slope was varied between $0 \leq \beta/\beta_r \leq 0.95$, and a selection of artificial sediments were used with grain sizes ranging from 0.08 mm to 1.1 mm (corresponding to hydraulically smooth or transitional regimes). In this case, values of $\hat{u}_{b,c}/\hat{u}_{b,c,0}$ were reported, where $\hat{u}_{b,c}$ was taken to be the peak tangential flow speed measured adjacent to the bed surface during the interaction, and were found to exhibit a very good degree of correspondence with the rhs of Eq. (11) for the sediment layers consisting of grains with sizes less than 0.4 mm, and with the rhs of Eq. (10) for the larger sediment types. Unlike the data reported in Lamb *et al.*[14]—which, recall, were found to be affected by the decrease in flow depth that occurs in an open-channel flow when the channel slope is notably increased—the configurations used by Chiew and Parker[16] and Munro[17] allowed the fluid depth to remain fixed for all bed slopes and, as a result, their results exhibit a clear agreement with the trend of increased mobility with increasing bed slope, predicted by the theory. Likewise, the fluid depth was fixed in the configuration used in this study, and so a similar trend was anticipated.

Figure 5 shows the measured values of $\langle \hat{u} \rangle_{c,\beta}/\langle \hat{u} \rangle_{c,0}$ (which, recall, are also given in Table II) plotted against normalised bed slope β/β_r. As in Fig. 4, each sediment type is represented by a different data symbol (see caption for details). To promote straightforward comparison, the data have been plotted on the same semi-log-scale axes used by both Chiew and Parker[16] and Munro.[17] The theoretical relationships defined in Eqs. (10) and (11), which correspond, respectively, to the hydraulically rough and hydraulically smooth cases, are also shown, by the broken and solid lines,

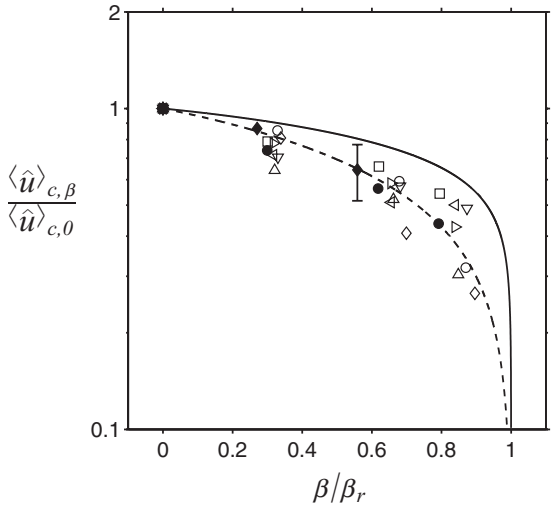

FIG. 5. Measured values of the normalised, near-bed peak rms horizontal velocity component, $\langle \hat{u} \rangle_{c,\beta}/\langle \hat{u} \rangle_{c,0}$, plotted against normalised bed slope β/β_r, for each of the nine sediment types: A (◊), B (○), C (△), D (▽), E (□), F (▷), G (◁), H (●), and I (♦). For comparison, Eqs. (10) and (11) are shown, respectively, by the broken and solid lines. To avoid saturation, a single error bar has been included that is representative of the variability observed in all data shown.

and have been evaluated using $\phi_r = 29.4^\circ$, which is the mean of the repose angles listed in Table II. Hence, here, one would expect the data to fall either on, or in the region between the two lines defined by Eqs. (10) and (11), as was the case for the data reported by Munro.[17] Despite the noticeable scatter evident within the data, Fig. 5 confirms that, for the nine sediment types considered here, the bed mobility is observed to increase with bed slope. Moreover, all data are generally in better correspondence with the rough-flow regime defined in Eq. (10) (broken line) or with the transitional region between Eqs. (10) and (11), in spite of the fact that sediment types E, F, G, and I (with $D_{50} \lesssim 0.3$ mm) are traditionally associated with the hydraulically smooth regime. This is notably different from the data reported in Munro,[17] where the corresponding measurements of the normalised near-bed peak velocities ($\hat{u}_{b,c}/\hat{u}_{b,c,0}$) were in very good agreement with the rhs of (11) for those sediments with $D_{50} \lesssim 0.3$ mm.

One possible reason for the trend observed in Fig. 5 is that the structure of the turbulence, which recall consists of dominant fluctuating components superimposed on a weaker, secondary mean flow (see Fig. 3), inhibits the formation of a "traditional" viscous-sublayer structure. Note, however, that this assertion is not supported by the data shown in Fig. 4, where the monotonic increase in $\theta_{c,0}$ with decreasing Re_p suggests that the damping effect of viscous stresses, typically associated with the presence of a viscous sublayer, is evident for the smaller sediment types. However, as noted by Wiberg and Smith,[15] even if a viscous sublayer does form its structure is likely to be continually depressed (and expanded) by energetic turbulent eddies either present near the bed, or directly interacting with the bed. One would certainly expect this to be the case for the flow considered here. Indeed, energetic turbulent eddies (or, more precisely, coherent vortex structures) interacting with sediment layers in steady channel flows have been shown[9,10] to cause significant localised disruption of the viscous sublayer, leading to notable increases in the magnitude of the local bed shear stress. Under such conditions, and even for a bedform normally associated with the hydraulically smooth regime, one might expect the conditions used to derive Eq. (10), rather than those used to derive Eq. (11), to be valid in these local "disrupted" regions.

IV. SUMMARY AND FINAL REMARKS

In this paper, we have reported measurements of sediment threshold criteria taken in the presence of oscillating-grid turbulence, using a set of nine mono-disperse artificial sediments with diameters ranging from 0.08 mm to 1.09 mm (size ranges normally associated with either hydraulically smooth beds or transitional flow). Attention was focussed on analysing how the threshold criteria were affected by increases in bed slope between $0 \leq \beta \leq \beta_r$. To achieve this, the apparatus were designed so that the oscillating-grid mechanism and sediment layer could be tilted simultaneously, so that the spanwise plane of the grid could be kept parallel to the sediment-layer surface. Time-resolved two-dimensional PIV was used to measure the fluid velocity field in the vertical mid-plane of the tank, in the region between the grid and the bedform's surface. Statistical analysis of the velocity data showed that (a) the mean flow components were secondary compared to the fluctuations, and that (b) the grid-generated turbulence had an anisotropic structure, due to the relative close proximity of the grid to the sediment layer. [This is notably different from most OGT studies where the grid is positioned so that tank base (or lid) has little influence on the flow, resulting in the production of quasi-isotropic turbulence within the bulk fluid.] In particular, it was shown that when the turbulence interacts with the bedform their is a net transfer of energy from the normal to the tangential velocity components, which gives rise to a peak in the tangential rms velocity component in the region just above the bed surface. The sediment threshold criteria were analysed in terms of a modified Shields[1] parameter, $\theta_{c,\beta}$, defined in terms of this near-bed peak tangential velocity scale.

Measurements of $\theta_{c,0}$ (for horizontal bedforms) were plotted against Re_p and compared with the standard Shields[1] curve. Although the data were a factor of two greater than the predicted values, there was clear qualitative agreement between the data trend and that predicted by the Shields[1] curve for the range of Re_p considered here. The effects of bed slope were analysed by comparing the measured values of $\langle\hat{u}\rangle_{c,\beta}/\langle\hat{u}\rangle_{c,0} = (\theta_{c,\beta}/\theta_{c,0})^{1/2}$ for each normalised bed slope β/β_r with the theoretical models reported previously by Chiew and Parker[16] (for hydraulically rough beds) and Munro[17] (for hydraulically smooth beds). In all cases, the bed mobility was found to increase with bed

slope. However, despite the fact that the grain sizes used here correspond to either the hydraulically smooth, or transitional regimes, the measured values of $\langle\hat{u}\rangle_{c,\beta}/\langle\hat{u}\rangle_{c,0}$ for each of the nine sediment types were, within general scatter, best described by the theoretical model based on the conditions for hydraulically rough beds (Eq. (10)). We believe this result is due to how turbulence interacting with a bedform can act to distort the structure of the viscous sublayer that may form adjacent to the bed surface. That is, an energetic eddy interacting with the bedform produces localised regions of intense vortical fluid immediately above the bed surface which may disrupt (or thin) the sublayer structure, exposing the local near surface sediment grains to increased drag and lift forces. Under such conditions, provided the interaction is sufficiently energetic, the local peak bed shear stress is likely to scale as $\rho\langle\hat{u}\rangle^2_{c,\beta}$ which, recall, is the condition used in the derivation of Eq. (10).

Further experimental study of the interaction between OGT and a sediment layer is currently ongoing. These experiments focus on two different aspects. First, a combination of two-dimensional PIV applied to the bed surface (using tracer grains within the sediment)[17] and laser Doppler velocimetry applied to the fluid, are being used to measure the correlation between the near-bed turbulence and the velocities of sediment grains brought into motion by the interaction. Second, a light attenuation technique[32] is being used to obtained accurate, spatially-resolved measurements of sediment erosion levels induced by OGT. These results will be reported subsequently.

ACKNOWLEDGMENTS

This work was funded by the Engineering and Physical Sciences Research Council (Grant No. EP/H007032/1). The authors gratefully acknowledge Pablo Vivero for assisting with the experimental work, and for the technical support provided by Damien Goy.

[1] A. Shields, "Anwendung der Ahnlichkeitsmechanik und der turbulenzforschung auf die geschiebebewegung," Preussiche Versuchsansalt für Wasserbrau und Schiftbrau **26**, 26 (1936).
[2] C. M. White, "The equilibrium of grains in the bed of a stream," Proc. R. Soc. London, Ser. A **174**, 322–338 (1940).
[3] S. J. White, "Plane bed thresholds for fine grained sediments," Nature (London) **228**, 152–153 (1970).
[4] Y. Niño, F. Lopez, and M. Garcia, "Threshold for particle entrainment into suspension," Sedimentology **50**, 247–263 (2003).
[5] W. R. Brownlie, "Flow depth in sand-bed channels," J. Hydraul. Eng. **109**(7), 959–990 (1983).
[6] J. M. Nelson, S. R. Mclean, and S. R. Wolfe, "Mean flow and turbulence fields over two-dimensional bed forms," Water Resour. Res. **29**, 3935–3953, doi:10.1029/93WR01932 (1993).
[7] J. M. Nelson, R. L. Shreve, S. R. Mclean, and T. G. Drake, "Role of near-bed turbulence structure in bed load transport and bed form mechanics," Water Resour. Res. **31**, 2071–2086, doi:10.1029/95WR00976 (1995).
[8] B. M. Sumer, L. H. C. Chua, N. S. Cheng, and J. Fredsøe, "The influence of turbulence on bedload sediment transport," J. Hydraul. Eng. **129**, 585–596 (2003).
[9] Y. Niño and M. H. Garcia, "Experiments on particle-turbulence interactions in the near-wall region of an open channel flow: Implications for sediment transport," J. Fluid Mech. **326**, 285–319 (1996).
[10] D. Kaftori, G. Hetsroni, and S. Banerjee, "Particle behaviour in the turbulent boundary layer. I. Motion, deposition, and entrainment," Phys. Fluids **7**, 1095–1106 (1995).
[11] D. Kaftori, G. Hetsroni, and S. Banerjee, "Particle behaviour in the turbulent boundary layer. II. Velocity and distribution profiles," Phys. Fluids **7**, 1107–1121 (1995).
[12] R. J. Munro, N. Bethke, and S. B. Dalziel, "Sediment resuspension and erosion by vortex rings," Phys. Fluids **21**, 046601 (2009).
[13] M. W. Schmeeckle, J. M. Nelson, and R. L. Shreve, "Forces on stationary particles in near-bed turbulent flows," J. Geophys. Res. **112**, F02003, doi:10.1029/2006JF000536 (2007).
[14] M. P. Lamb, W. E. Dietrich, and J. G. Venditti, "Is the critical Shields stress for incipient sediment motion dependent on channel-bed slope," J. Geophys. Res. **113**, F02008, doi:10.1029/2007JF000831 (2008).
[15] P. L. Wiberg and J. D. Smith, "Calculations of the critical shear stress for motion of uniform and heterogeneous sediments," Water Resour. Res. **23**(8), 1471–1480, doi:10.1029/WR023i008p01471 (1987).
[16] Y.-M. Chiew and G. Parker, "Incipient sediment motion on non-horizontal slopes," J. Hydraul. Res. **32**, 649–660 (1994).
[17] R. J. Munro, "The interaction of a vortex ring with a sloped sediment layer: Critical criteria for incipient grain motion," Phys. Fluids **24**, 026604 (2012).
[18] R. A. Bagnold, "Motion of waves in shallow water: Interaction between waves and sand bottoms," Proc. R. Soc. London **187**, 1–15 (1946).
[19] P. D. Komar and M. C. Miller, "The threshold of sediment movement under oscillatory water waves," J. Sediment. Petrol. **43**(4), 1101–1110 (1973).
[20] R. R. Long, "Theory of turbulence in a homogeneous fluid induced by an oscillating grid," Phys. Fluids **21**(10), 1887–1888 (1978).

[21] I. P. D. De Silva and H. J. S. Fernando, "Oscillating grids as a source of nearly isotropic turbulence," Phys. Fluids **6**(7), 2455–2464 (1994).
[22] S. M. Thompson and J. S. Turner, "Mixing across an interface due to turbulence generated by an oscillating grid," J. Fluid Mech. **67**, 349–368 (1975).
[23] E. J. Hopfinger and J. A. Toly, "Spatially decaying turbulence and its relation to mixing across density interfaces," J. Fluid Mech. **78**, 155–175 (1976).
[24] H. E. Huppert, J. S. Turner, and M. A. Hallworth, "Sedimentation and entrainment in dense layers of suspended particles stirred by an oscillating grid," J. Fluid Mech. **289**, 263–293 (1995).
[25] J. J. Orlins and J. S. Gulliver, "Turbulence quantification and sediment resuspension in an oscillating grid chamber," Exp. Fluids **34**, 662–677 (2003).
[26] P. Medina, M. A. Sánchez, and J. M. Redondo, "Grid stirred turbulence: Applications to the initiation of sediment motion and lift-off studies," Phys. Chem. Earth, Part B **26**(4), 299−304 (2001).
[27] M. Belinsky, H. Rubin, Y. Agnon, E. Kit, and J. F. Atkinson, "Characteristics of resuspension, settling and diffusion of particulate matter in a water column," Environ. Fluid Mech. **5**, 415−441 (2005).
[28] H. J. S. Fernando and I. P. D De Silva, "Note on secondary flows in oscillating-grid, mixing-box experiments," Phys. Fluids **5**(7), 1849–1851 (1993).
[29] E. Kit, E. J. Strang, and H. J. S. Fernando, "Measurements of turbulence near shear-free density interfaces," J. Fluid Mech. **334**, 293–314 (1997).
[30] T. Uzkan and W. C. Reynolds, "A shear-free turbulent boundary layer," J. Fluid Mech. **28**, 803–821 (1967).
[31] B. Perot and P. Moin, "Shear-free turbulent boundary layers. Part 1. Physical insights into near-wall turbulence," J. Fluid Mech. **295**, 199–227 (1995).
[32] R. J. Munro and S. B. Dalziel, "Attenuation technique for measuring sediment displacement levels," Exp. Fluids **39**, 602–613 (2005).